

# A mixture theory for size and density segregation in shallow granular free-surface flows

D. R. Tunuguntla<sup>1,2,†</sup>, O. Bokhove<sup>1,3</sup> and A. R. Thornton<sup>1,2</sup>

<sup>1</sup>Mathematics of Computational Science group, University of Twente, The Netherlands

<sup>2</sup>Multi-Scale Mechanics group, MESA+, University of Twente, The Netherlands

<sup>3</sup>School of Mathematics, University of Leeds, UK

(Received 15 September 2013; revised 3 March 2014; accepted 17 April 2014)

In the past ten years much work has been undertaken on developing mixture theory continuum models to describe kinetic sieving-driven size segregation. We propose an extension to these models that allows their application to bidisperse flows over inclined channels, with particles varying in density and size. Our model incorporates both a recently proposed explicit formula for how the total pressure is distributed among different species of particles, which is one of the key elements of mixture theory-based kinetic sieving models, and a shear rate-dependent drag. The resulting model is used to predict the range of particle sizes and densities for which the mixture segregates. The prediction of no segregation in the model is benchmarked by using discrete particle simulations, and good agreement is found when a single fitting parameter is used which determines whether the pressure scales with the diameter, surface area or volume of the particle.

**Key words:** granular media, granular segregation

---

## 1. Introduction

When free-surface granular flows with particles differing in size and/or density discharge down an inclined plane, they often segregate to form complex patterns (Drahn & Bridgwater 1983; Khakhar, McCarthy & Ottino 1999). These flow-induced effects must often be avoided in production processes of the pharmaceutical, chemical, food, steel and cement industries (Shinbrot, Alexander & Muzzio 1999; Duran 2000). Therefore, a quantitative prediction of segregation is vital to improving product quality and the design of the material-handling equipment. Despite its importance, the fundamentals of this phenomenon are incompletely understood.

In general, segregation or demixing occurs because of differences in particle properties such as size (Wiederseiner *et al.* 2011), density (Tripathi & Khakhar 2013), shape (Pollard & Henein 1989), inelasticity (Brito & Soto 2009), surface roughness and friction (Ulrich, Schröter & Swinney 2007). Differences in size and density are the primary factors affecting demixing in free-surface flows over inclined channels.

† Email address for correspondence: [d.r.tunuguntla@utwente.nl](mailto:d.r.tunuguntla@utwente.nl)

Experimental studies have been performed to examine the combined effects of size and density differences (Felix & Thomas 2004; Jain, Ottino & Lueptow 2005), but few continuum models have considered these combined effects (Marks, Rognon & Einav 2012). Felix & Thomas (2004) experimentally analysed the size and density effects of particles in bidisperse mixture flows in rotating tumblers, over inclined channels and pile formations. Using a continuum approach, we present an analysis that predicts the degree of segregation in a bidisperse mixture flow over inclined channels, due to both size and density differences. The zero-segregation prediction from our continuum model is later benchmarked against discrete particle simulations.

Among several mechanisms that could cause segregation (Bridgwater 1976), our focus is on kinetic sieving, which is the dominant mechanism causing segregation in gravity-driven free-surface flows, when the size ratio is less than 2 (Savage & Lun 1988). For size ratios greater than 2, percolation effects become important and should be included in the model (Savage & Lun 1988; Thornton *et al.* 2012). We use the framework of mixture theory (e.g. Morland 1992) and extend the ideas of Gray & Thornton (2005) and Thornton, Gray & Hogg (2006) in two ways: (i) we relax the assumption of equal particle-species density; (ii) we incorporate a shear rate-dependent interspecies drag with a slightly more general pressure scaling function than that proposed by Marks *et al.* (2012). The resulting theory is able to predict the range of sizes and densities for which segregation will occur directly from the known particle size and density. Previously Marks *et al.* (2012) stated a way to incorporate density differences, but they did not consider these combined effects in detail.

## 2. Particle segregation model

We choose a domain consisting of a chute inclined at a constant angle  $\theta$  to the horizontal and a Cartesian coordinate system in which the  $x$ -axis points down the chute, the  $y$ -axis points across its width and the  $z$ -axis points in the upward direction normal to the chute.

### 2.1. Mixture framework

Our starting point for the model is a granular mixture theory composed of two different constituents, indexed by 1 and 2 and referred to as species type 1 and species type 2, whose interstitial pore space is filled with air, which has a negligible effect on these dense granular flows. Mixture theory (e.g. Morland 1992) for a binary continuum postulates that all constituents of the mixture simultaneously occupy space and time. This leads to overlapping fields with partial pressures  $p^v$ , densities  $\rho^v$  and velocities  $\mathbf{u}^v = [u^v, v^v, w^v]^T$  in the three coordinate directions corresponding to each constituent, indexed by  $v = 1, 2$ . Each constituent satisfies the following fundamental balance laws of mass and momentum for these partial fields:

$$\partial_t \rho^v + \nabla \cdot (\rho^v \mathbf{u}^v) = 0, \quad (2.1a)$$

$$\rho^v (\partial_t \mathbf{u}^v + \mathbf{u}^v \cdot \nabla \mathbf{u}^v) = -\nabla p^v + \rho^v \mathbf{g} + \beta^v, \quad (2.1b)$$

where  $\mathbf{g} = (g_t, 0, -g_n)^T$  is the gravity vector, with  $g$  being the standard acceleration due to free fall, such that  $g_t = g \sin \theta$  and  $g_n = g \cos \theta$ . The  $\beta^v$  represent interspecies drag forces that resist the motion between constituents. As these forces are internal, by Newton's third law the sum of these drags must be zero, i.e.  $\beta^1 + \beta^2 = \mathbf{0}$ . Given a unit mixture volume, each of the constituents occupies a volume fraction  $\phi^1$  or  $\phi^2$ , including the interstitial pore space. Hence, by definition, the individual volume

fractions sum to unity,  $\phi^1 + \phi^2 = 1$ . Furthermore, the bulk density  $\rho$ , barycentric granular velocity or bulk velocity  $\mathbf{u}$  and bulk pressure  $p$  are defined as  $\rho = \rho^1 + \rho^2$ ,  $\mathbf{u} = (\rho^1 \mathbf{u}^1 + \rho^2 \mathbf{u}^2) / \rho$  and  $p = p^1 + p^2$ , respectively. A vital element in the mixture theory is the relation between partial and intrinsic variables, whereby variables such as velocity, density and pressure are related as follows:

$$\mathbf{u}^v = \mathbf{u}^{v*}, \quad \rho^v = \phi^v \rho^{v*}, \quad p^v = \phi^v p^{v*} \quad \text{with } p^{v*} = f^v p, \quad (2.2a-c)$$

where ‘\*’ indicates when a variable is intrinsic. Motivated by Marks *et al.* (2012), we assume that  $f^v$  scales with the species size  $s^v$  as

$$f^v = \frac{(s^v)^a}{\sum (s^v)^a \phi^v} \quad (2.3)$$

for  $v = 1, 2$  and  $a > 0$ . The new definition for partial pressure, (2.2c), is a slight generalisation of the form used by Marks *et al.* (2012). When  $a = 1, 2$  or  $3$ , the pressure scales precisely with the length, surface area or volume of the particle, respectively.

### 2.1.1. Drag force

In a simple shear flow of a mixture with different particle species, the shear causes the species to preferentially fall into the gaps created beneath them (kinetic sieving) or to rise upwards through each other (squeeze expulsion), resulting in interspecies friction (Savage & Lun 1988). Following Marks *et al.* (2012), a generalised version of the Gray & Thornton (2005) interaction drag or interspecies friction is assumed to be

$$\beta^v = p \nabla (\phi^v f^v) - \rho^v \frac{c}{\dot{\gamma}} (\mathbf{u}^v - \mathbf{u}) \quad (v = 1, 2), \quad (2.4)$$

where  $c$  is an *a priori* unknown coefficient of interspecies interaction and  $\dot{\gamma}$  is the shear rate. Note that  $c/\dot{\gamma}$  has dimension  $s^{-1}$ . The momentum balance for each individual species, (2.1b), can be thus restated as

$$\rho^v (\partial_t \mathbf{u}^v + \mathbf{u}^v \cdot \nabla \mathbf{u}^v) = -\phi^v f^v \nabla p + \rho^v \mathbf{g} - \rho^v \frac{c}{\dot{\gamma}} (\mathbf{u}^v - \mathbf{u}). \quad (2.5)$$

In shallow large-scale industrial or natural granular flows, the aspect ratio of velocity and flow length scales in the downslope and cross-slope directions to those in the normal direction is small. Summing the momentum balance equation (2.5) of each species implies that the flow at leading order in this aspect ratio is in lithostatic balance, i.e.  $\partial p / \partial z = -\rho g \cos \theta$ . Moreover, the downslope and cross-slope velocities of the species are considered to be equal to the bulk downslope and cross-slope velocity components, i.e.  $u^v = u$  and  $v^v = v$  for  $v = 1, 2$ . Assuming the flow to be in viscous balance by neglecting the inertia terms, and substituting the drag force and velocity definitions into the particles’ normal momentum balance equation, the species percolation or normal velocity is found to be

$$w^1 = w - \frac{g_n}{c} \dot{\gamma} \left[ \frac{(1 - \phi)(\widehat{s}^a - \widehat{\rho})}{\phi + (1 - \phi)\widehat{s}^a} \right], \quad w^2 = w + \frac{g_n}{c} \dot{\gamma} \frac{1}{\widehat{\rho}} \left[ \frac{\phi(\widehat{s}^a - \widehat{\rho})}{\phi + (1 - \phi)\widehat{s}^a} \right]. \quad (2.6a,b)$$

Here  $\hat{\rho} = \rho^{2*}/\rho^{1*}$  and  $\hat{s} = s^2/s^1$  are the particle density and size ratios, respectively, whereas  $\phi = \phi^1$  is the volume fraction of species type 1. By combining the mass balance equation (2.1a) and the percolation velocity (2.6a), we obtain the governing equation for  $\phi^1 = \phi$  as

$$\frac{\partial \phi}{\partial t} + \frac{\partial(\phi u)}{\partial x} + \frac{\partial(\phi v)}{\partial y} + \frac{\partial(\phi w)}{\partial z} - \frac{\partial}{\partial z} \left( \frac{g_n}{c} \dot{\gamma} (\hat{s}^a - \hat{\rho}) \left[ \frac{\phi(1-\phi)}{\phi + (1-\phi)\hat{s}^a} \right] \right) = 0. \quad (2.7)$$

In general, an approximate bulk velocity  $\mathbf{u} = (u, v, w)^T$  can be computed from an existing shallow granular model (e.g. Grigorian, Eglit & Iakimov 1967; Savage & Hutter 1991; Bokhove & Thornton 2012), and then a fully coupled model can be developed. An example of how to couple these types of models can be found in Woodhouse *et al.* (2012), where a coupled model to describe the geophysically important granular fingering instability is derived.

### 2.1.2. Scaling

Assuming the bulk flow velocity is approximated using such models, the flow quantities are scaled as follows:

$$(x, y, z) = (L\tilde{x}, L\tilde{y}, H\tilde{z}), \quad (u, v, w) = (U\tilde{u}, U\tilde{v}, (HU/L)\tilde{w}), \quad t = (L/U)\tilde{t}. \quad (2.8a-c)$$

The variables  $U$ ,  $L$  and  $H$  are suitable characteristic scales for the flow velocity, length and depth/height, respectively, where  $L \gg H$ . Substituting the above scalings and dropping tildes, the governing equation (2.7) is restated as

$$\frac{\partial \phi}{\partial t} + \frac{\partial(\phi u)}{\partial x} + \frac{\partial(\phi v)}{\partial y} + \frac{\partial(\phi w)}{\partial z} - \frac{\partial}{\partial z} \left[ \hat{S}_r F(\phi) \right] = 0 \quad \text{with } F(\phi) = \left[ \frac{\phi(1-\phi)}{\phi + (1-\phi)\hat{s}^a} \right], \quad (2.9)$$

where  $\hat{S}_r = qL/(HU)$  is the non-dimensional number defined as the ratio of the mean segregation velocity,  $q = \frac{g_n}{c} (\hat{s}^a - \hat{\rho}) \dot{\gamma}$ , to a typical magnitude of the normal bulk velocity.

## 3. Solutions for limiting cases

For the kinematic limiting cases, solutions to (2.9) are constructed for a velocity field  $\mathbf{u} = (u(z), 0, 0)$  in the domain  $0 \leq z \leq 1$  and  $x \geq 0$ , for a mixture flow of unit height. For simplicity, initially we consider thin or shallow flows in which the velocity profiles are almost linear (Weinhart *et al.* 2012); hence, to a good approximation, we can take the shear rate  $\dot{\gamma}$  to be constant. For the case with  $\hat{S}_r = \bar{S}_r$  constant, (2.9) becomes

$$\frac{\partial \phi}{\partial t} + u \frac{\partial \phi}{\partial x} - \bar{S}_r \frac{\partial}{\partial z} \left( \frac{\phi(1-\phi)}{\phi + (1-\phi)\hat{s}^a} \right) = 0. \quad (3.1)$$

As in Gray & Thornton (2005), we use a simplified boundary condition with no flux of particles at the free surface and the base by considering  $F(\phi) = 0$  at  $z = 0, 1$ . Solutions to (3.1) can be constructed for two types of inflow boundary conditions, prescribed at  $x=0$ , termed homogeneous mixture inflow and normally graded mixture inflow. In the former case, a homogeneous mixture of concentration with  $\phi(0, z, t) = \phi_0$ , a constant, enters at  $x=0$ ; in the latter case, normally graded particles, i.e. a mixture in which smaller particles lie on top of the larger particles, enters at  $x=0$ .

### 3.1. Analytical solutions

Assuming that the flow has reached its steady state, the differential equation (3.1) is restated as

$$u(z) \frac{\partial \phi}{\partial x} - \bar{S}_r \left[ \frac{(\phi - 1)^2 \hat{s}^a - \phi^2}{(\phi + (1 - \phi) \hat{s}^a)^2} \right] \frac{\partial \phi}{\partial z} = 0, \quad (3.2)$$

which is a quasilinear partial differential equation. By using the method of characteristics, as applied in Gray & Thornton (2005) and Thornton *et al.* (2006), (3.2) above is analytically solved for specific inflow boundary conditions.

#### 3.1.1. Characteristics

An exact solution to the above equation is obtained via the method of characteristics, such that  $\phi$  is constant,  $\phi_\lambda$ , along each characteristic curve given by

$$u(z) \frac{dz}{dx} = \bar{S}_r \left[ \frac{(\phi_\lambda - 1)^2 \hat{s}^a - \phi_\lambda^2}{(\phi_\lambda + (1 - \phi_\lambda) \hat{s}^a)^2} \right]. \quad (3.3)$$

The characteristics describe the flux of information into the domain. Given a velocity field  $u(z)$ , the above equation is integrable as the downslope velocity  $u$  is a function of  $z$  alone and  $\phi_\lambda$  is constant. Solutions for general velocity fields can be obtained by introducing a depth-integrated velocity coordinate  $\psi$ , where

$$\psi = \int_0^z u(z') dz'. \quad (3.4)$$

Equation (3.3) can then be integrated to give straight-line characteristics

$$\psi = \bar{S}_r \left[ \frac{(\phi_\lambda - 1)^2 \hat{s}^a - \phi_\lambda^2}{(\phi_\lambda + (1 - \phi_\lambda) \hat{s}^a)^2} \right] (x - x_\lambda) + \psi_\lambda \quad (3.5)$$

in terms of the mapped variables, with  $(x_\lambda, \psi_\lambda)$  as the starting point for varying  $\phi_\lambda$ . We choose a scaling such that without loss of generality the mapped coordinate  $\psi$  equals 1 at the free surface  $z = 1$ . As we take  $u(z) > 0$  from the outset to simplify matters, the map between the physical and depth-integrated coordinates can easily be constructed for a whole class of general velocity fields.

#### 3.1.2. Jump conditions

Experimental evidence of segregating flows reveals that concentration jumps or shocks can emerge (Savage & Lun 1988). The presence of shocks implies that the segregation equation (2.9) or (3.1) is no longer valid because the particle concentration  $\phi$  is then no longer continuous. Hence, a jump condition should be applied across the discontinuity (Whitham 1974). We derive the jump condition from an integral version of the conservative form of the segregation equation (3.1). We have

$$\frac{\partial}{\partial x} \int_{L_2}^{L_1} \phi u dz - \bar{S}_r \left[ \frac{\phi(1 - \phi)}{\phi + (1 - \phi) \hat{s}^a} \right]_{L_1}^{L_2} = 0. \quad (3.6)$$

Assuming that a jump in  $\phi$  exists at  $z = J(x)$ , and following Whitham (1974), the jump condition is

$$\left[ \phi u J' + \bar{S}_r \left( \frac{\phi(1 - \phi)}{\phi + (1 - \phi) \hat{s}^a} \right) \right]_-^+ = 0, \quad (3.7)$$

where  $J' = dJ/dx$ ,  $+$  and  $-$  denote the limits on either side of the discontinuity or jump  $J(x)$  and square brackets  $[ ]$  denote the difference of the enclosed function value at the upper and lower limits. Since  $u(z)$  is continuous, the above equation can be restated as

$$u \frac{dJ}{dx} = -\bar{S}_r \left( \frac{(1 - (\phi^+ + \phi^-))\hat{s}^a - \phi^+\phi^-(1 - \hat{s}^a)}{\phi^+\phi^-(\hat{s}^a - 1)^2 + (\phi^+ + \phi^-)(\hat{s}^a - \hat{s}^{2a}) + \hat{s}^{2a}} \right), \quad (3.8)$$

which, when solved, gives the location,  $z = J(x)$ , of the shock. Following Gray & Thornton (2005), we restate the above equation in terms of depth-integrated velocity coordinates (3.4), i.e.

$$\frac{d\psi_J}{dx} = -\bar{S}_r \left( \frac{(1 - (\phi^+ + \phi^-))\hat{s}^a - \phi^+\phi^-(1 - \hat{s}^a)}{\phi^+\phi^-(\hat{s}^a - 1)^2 + (\phi^+ + \phi^-)(\hat{s}^a - \hat{s}^{2a}) + \hat{s}^{2a}} \right), \quad (3.9)$$

independent of the assumed monotonically increasing velocity profile, with  $\psi_J = \psi(J(x))$ .

### 3.1.3. Jumps in mapped coordinates

For a homogeneous inflow condition and purely size-based segregation, i.e.  $\hat{\rho} = 1$ , the positions of the shocks are determined from the shock relations (3.9). By substituting  $\phi^+ = 1$  and  $\phi^- = \phi_0$  and integrating with the boundary condition  $\psi = 0$  at  $x = 0$ , the position of one shock is obtained as  $\psi_1 = -(g_n/c)(1 - \hat{s}^a)[\phi_0/(\phi_0 + (1 - \phi_0)\hat{s}^a)]x$ . Similarly, by substituting  $\phi^+ = 0$  and  $\phi^- = \phi_0$  into the shock relations and integrating with the boundary condition  $\psi = 1$  at  $x = 0$ , the position of another shock is obtained as  $\psi_2 = 1 + (g_n/c)(1 - \hat{s}^a)[(1 - \phi_0)(\phi_0 + (1 - \phi_0)\hat{s}^a)]x$ . The shock  $\psi_2$  propagates downwards to merge with shock  $\psi_1$  at the triple point  $x_{triple} = (\phi_0 + (1 - \phi_0)\hat{s}^a)((\hat{s}^a - 1)(g_n/c))$  and at  $\psi = \phi_0$  in depth-integrated velocity variables, resulting in a third shock that separates the 100% species type 1 and species type 2 regions. The new shock position,  $\psi_3$ , is determined by substituting  $\phi^+ = 0$  and  $\phi^- = 1$  into the shock relations, which upon integrating gives  $\psi_3 = \phi_0$  for  $x \geq x_{triple}$ . When the shock positions  $\psi_1$ ,  $\psi_2$  and  $\psi_3$  are mapped back to physical coordinates, they yield the solid lines in figure 1.

### 3.1.4. Physical solutions and comparison with other models

The shock positions, in terms of the depth-integrated velocity coordinates, are valid for all velocity fields, given that the fields have a well-defined map from the depth-integrated velocity coordinate space to physical coordinate space. If we consider a linear shear profile  $u = \alpha + 2(1 - \alpha)z$  where  $0 \leq \alpha \leq 1$ , then it follows from (3.4) that the depth-integrated velocity coordinate satisfies  $\psi = \alpha z + (1 - \alpha)z^2$  with  $\psi(1) = 1$  at the free surface. The  $\psi$ -coordinate can easily be mapped back to physical space via

$$z = \begin{cases} \psi & \text{for } \alpha = 1, \\ \frac{-\alpha + \sqrt{\alpha^2 + 4(1 - \alpha)\psi}}{2(1 - \alpha)} & \text{for } \alpha \neq 1. \end{cases} \quad (3.10)$$

In the case of a simple shear flow where  $\alpha = 0$ , from (3.10) we find that  $z = \sqrt{\psi}$ , and thereby the jump/shock positions are mapped back to the physical space. Figure 1 shows the results from our model, the model of Gray & Thornton (2005) and the model of Savage & Lun (1988). To allow direct comparison of the effects of the flux functions between our model and that of Gray & Thornton (2005), the segregation

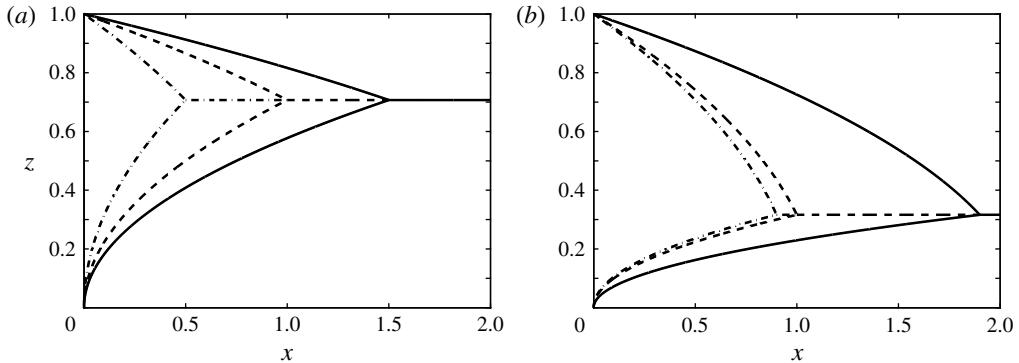


FIGURE 1. Comparison of analytical jump solutions for a simple shear flow ( $\alpha = 0$ ) and purely size-based segregation, obtained from the Savage and Lun theory (dot-dash lines), the Gray and Thornton theory (dashed lines) and our model with  $\hat{S}_r = 1$  and  $a = 1$  (solid lines). Note that to compare Gray and Thornton's model and our model, we take  $\bar{S}_r = 1$  in both theories. The panels show results for homogeneous inflow concentrations of (a)  $\phi_0 = 50\%$  and (b)  $\phi_0 = 10\%$ .

velocity,  $\bar{S}_r$ , is taken to be unity in both theories. Two things are clear from this comparison: firstly, the point of full segregation (location of the triple point) is further downstream for our model, by as much as a factor of 2 for  $\phi_0 = 0.1$ ; secondly, the distance to full segregation is a function of  $\phi_0$  in our model (in contrast to the model of Gray & Thornton 2005). Our flux function  $F(\phi)$  is convex and more general; it is apparent that the form of this function can have a large effect on the predicted distance to full segregation.

### 3.2. Numerical solutions

Solutions to the segregation equation (2.7) can be computed for various values of the shear  $\alpha$  and for constant and non-constant shear rates  $\dot{\gamma}$ . Following Marks *et al.* (2012), for sufficiently thick mixture flows we have

$$\dot{\gamma} = [(\tan \theta - \mu_c)/(k\bar{s})]\sqrt{1.5g \cos \theta H(1 - \bar{z})} \quad \text{where } \bar{s} = \sum \phi^v (s^v)^a \quad (v = 1, 2), \quad (3.11)$$

leading to a Bagnold-type velocity profile. Substituting (3.11) into the scaled segregation equation (2.9) and dropping tildes gives

$$\frac{\partial \phi}{\partial t} + \frac{\partial(\phi u)}{\partial x} + \frac{\partial(\phi v)}{\partial y} + \frac{\partial(\phi w)}{\partial z} - (\hat{s}^a - \hat{\rho}) M \frac{\partial}{\partial z} \left( \frac{\phi(1 - \phi)\sqrt{1 - \bar{z}}}{(\phi + (1 - \phi)\hat{s}^a)^2} \right) = 0, \quad (3.12)$$

where  $M = (L/HU)(g_n/c)(\tan \theta - \mu_c)\sqrt{1.5Hg \cos \theta}/k(s^1)^a$  is a material parameter,  $\mu_c$  is the friction coefficient and  $k$  is a non-dimensional constant when  $a = 1$  or a dimensional constant when  $a = 2$  or 3. Following (Marks *et al.* 2012), we choose  $M = 0.1$  implying that the discrete particle simulation and continuum numerical solution take the same time to reach steady state. We use a high-resolution shock-capturing method, the space discontinuous Galerkin finite element method (space-DGFEM) of Tassi, Bokhove & Vionnet (2007), implemented in our open-source DGFEM solver hpGEM (Pesch *et al.* 2007). Full details of the package, including

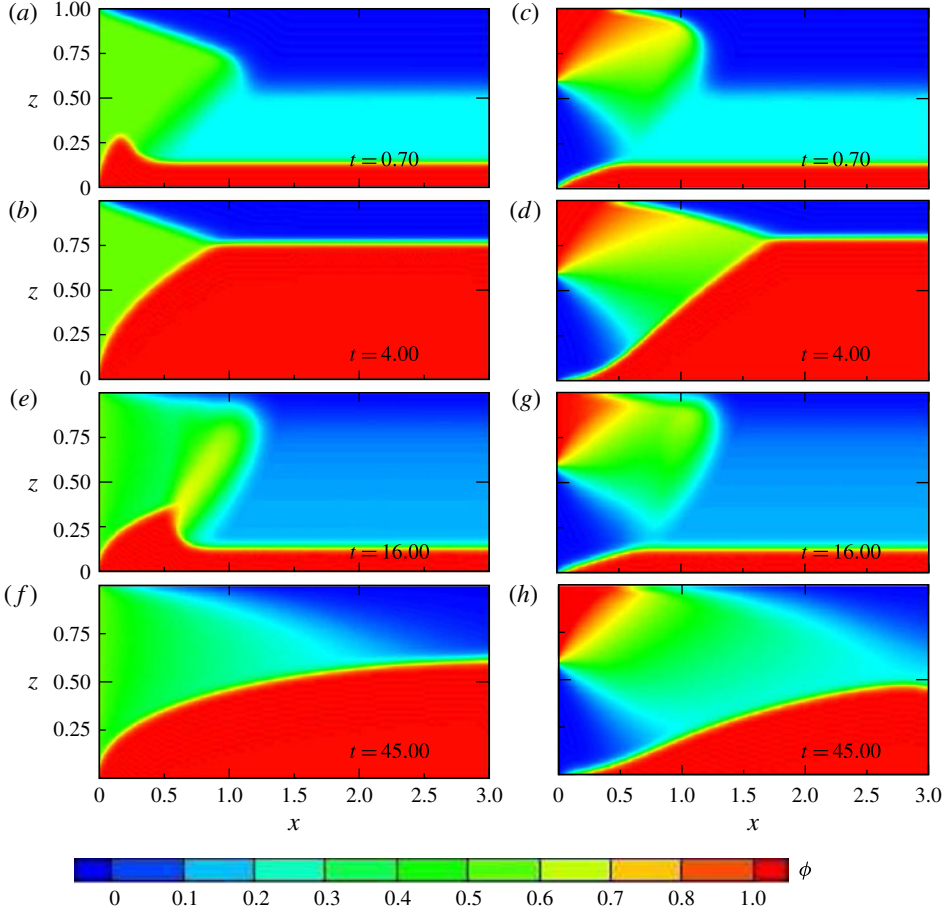


FIGURE 2. Development of the volume fraction  $\phi$  as a function of the downslope coordinate  $x$  and the flow depth  $z$ , when  $a=3$ ,  $\hat{\rho}=0.5$  and  $s=1.26$ ; the domain is initially filled with a mixture of  $\phi_1 = \phi(x, y, 0) = 0.25$ , and the bulk flow is from left to right. The number of elements is  $160 \times 60$ . The following two cases are shown: (i) constant shear rate  $\dot{\gamma} = 1$ , i.e. a simple shear flow ( $\alpha = 0$ ) with  $\hat{S}_r = 1.5$ , for (a,b) homogeneous mixture inflow ( $\phi_0 = 0.6$ ) and (c,d) normally graded mixture inflow; (ii) Bagnold-type shear rate (3.11) with  $M = 0.1$ , for (e,f) homogeneous mixture inflow ( $\phi_0 = 0.6$ ) and (g,h) normally graded mixture inflow.

the numerical codes used to generate figure 2, are available from the website [www.hpGEM.org](http://www.hpGEM.org). This new implementation of a DGFEM-based solver is accurate and robust and has been extensively tested against both the exact solutions and the solutions presented in Gray & Thornton (2005) and Thornton *et al.* (2006) for flux functions of the form  $F(\phi) = \phi(1 - \phi)$ .

Figure 2 shows the evolution to steady state, for homogeneous and normally graded inflow conditions, in the cases of (i) a constant shear rate  $\dot{\gamma} = 1$ , i.e. simple shear with  $\alpha = 0$ , and (ii) a Bagnold-type rate (3.11). For a constant shear rate,  $\dot{\gamma} = 1$ , and normally graded inflow, as shown in figure 2(c,d), the expected expansion fan and three-shock structure can be seen clearly (Thornton *et al.* 2006). On inspecting figure 2(a-d), it seems that the rational and convex flux function does not structurally



change the evolution of the solution when compared to the solutions in Gray & Thornton (2005) and Thornton *et al.* (2006); however, a full investigation of the dependence of the solution on this flux is beyond the scope of the present study. With a Bagnold-type shear rate, for both homogeneous and normally graded inflows, the upper shock as seen in figure 2(a–d) does not develop in figure 2(e)–(h); this is similar to what is captured by the cellular automata model of Marks & Einav (2011).

#### 4. No or weak segregation

One of the key new features of our model is its ability to predict the ratios of size and density for which no or very weak segregation would occur. Due to the non-dimensionalisation used, this is simply given by the line  $\hat{s}^a = \hat{\rho}$ ; recall that  $a = 1$  for the pressure function suggested by Marks *et al.* (2012).

To validate our no- or zero-segregation prediction, we used fully three-dimensional discrete particle method (DPM) simulations, also known as molecular dynamics (MD) or discrete element method (DEM) simulations, implemented in our own open-source DPM package MercuryDPM. This package has previously been used by Thornton *et al.* (2012) and Weinhart, Luding & Thornton (2013) to investigate size segregation in chute flows. Full details of MercuryDPM and the source code used for this paper can be found at the website [MercuryDPM.org](http://MercuryDPM.org).

##### 4.1. DPM simulation set-up

We simulate a homogeneously mixed bidisperse mixture of particles. We will refer to the two different types of particles as species type 1 and species type 2. In general, if  $d_i$  ( $i = 1, 2, \dots$ ) is defined as the particle diameter of species type  $i$ , then the mean particle diameter is

$$d_m = \sum_i \phi_i d_i, \quad (4.1)$$

with  $\phi_i$  being the volume fraction of particles of species type  $i$ . Hence, for a bidisperse mixture,  $d_m = \phi d_1 + (1 - \phi)d_2$  where  $\phi$  is the volume fraction of particles of species type 1. Correspondingly,  $\rho_m$  is the mean particle density.

In our chosen coordinate system, we consider a cuboidal box, periodic in  $x$  and  $y$ , inclined at  $26^\circ$  to the horizontal. The box has dimensions  $L \times W \times H = 20d_m \times 10d_m \times 10d_m$ . To create a rough base, we fill the box with a randomly distributed set of particles of both types of diameter  $d_m$  and simulate until a static layer of approximately 12 particles thick is produced. Then a slice of particles with centres at  $z \in [9.3, 11]d_m$  are fixed and translated 11 particle diameters downwards to form the base of the box. A solid flat wall is added below this layer of particles to ensure that none of the flow particles will fall through. Once the base is created, the box is inclined and filled with a homogeneously mixed bidisperse mixture; see figure 5 and Weinhart *et al.* (2012) for details.

The parameters in our DPM simulations are non-dimensionalised so that the mean particle diameter is  $\hat{d}_m = 1$ , the mass is  $\hat{m}_m = 1$  and the magnitude of gravity is  $\hat{g} = 1$ . Therefore the non-dimensional mean particle density is  $\hat{\rho}_m = \hat{m}_m/\hat{V}_m = 6/\pi$ , with mean particle volume  $\hat{V}_m = \pi(\hat{d}_m)^3/6$  and time scale  $\sqrt{\hat{d}_m/g}$ , where a hat indicates a non-dimensional quantity. Furthermore, given the diameters and densities of each species type, the particle size and density ratios,  $\hat{s}$  and  $\hat{\rho}$ , are defined as  $\hat{s} = d_2/d_1$  and  $\hat{\rho} = \rho_2/\rho_1$ .

The box is filled with a bidisperse mixture in which the number of particles of each type is

$$N_1 = \frac{\phi \widehat{V}_{box}}{(\widehat{d}_1)^3}, \quad N_2 = \frac{(1 - \phi) \widehat{V}_{box}}{(\widehat{d}_2)^3}, \quad (4.2a,b)$$

where  $\widehat{V}_{box} = 10 \times 20 \times 10$  is the volume of the box. The expressions in (4.2) ensure that the ratio of the total volume of species type 1 to the total volume of all the particles is  $\phi$  and that the dimensionless height of the flow,  $\widehat{H}$ , is the same for all simulations. Using (4.2) with homogeneous initial conditions (randomly mixed) and an initial particle volume fraction of  $\phi_i = 0.5$ , a series of DPM simulations for different values of  $\widehat{\rho}$  and  $\widehat{s}$  was carried out to make a  $[\widehat{\rho} \times \widehat{s}]$  phase plot.

For all the simulations performed, we used a linear spring dashpot model with a contact duration of  $t_c = 0.005 \sqrt{d_m/g}$ , coefficient of restitution  $r_c = 0.88$  and contact friction coefficient  $\mu_c = 0.5$ . More details about the contact model can be found in Cundall & Strack (1979), Luding (2008) and Weinhart *et al.* (2012).

#### 4.2. Analysis

The sensitivity to both basal and initial conditions of the steady state has been thoroughly investigated, and hardly any sensitivity was found (Te Voortwis 2013). Once the flow has reached its steady state, we calculate the relative difference between the centres of mass as a function of  $\widehat{s}$  and  $\widehat{\rho}$ ,  $\widehat{D}_{com}(\widehat{\rho}, \widehat{s}) = (COM_2 - COM_B)/COM_B$ . Here  $COM_2$  is the vertical centre of mass of type-2 particles and  $COM_B$  is the vertical centre of mass of the bulk. For a given  $\widehat{s}$  and  $\widehat{\rho}$ , the flow is steady when the function value  $\widehat{D}_{com}$  remains constant with time. In figure 4, we plot the values of  $\widehat{D}_{com}$  for given  $\widehat{\rho}$  and  $\widehat{s}$ . When the value of  $\widehat{D}_{com}$  is positive, particles of species type 2 are near the free surface; when it is negative, particles of species type 2 are near the base, as can be seen in figure 3. Close inspection of the data shows very weak segregation along the solid line  $\widehat{s}^a = \widehat{\rho}$  with  $a = 3$ , which also implies that the pressure is scaled by the volume of the particle. Below the solid line the type-2 particles rise towards the free surface, and above the solid line the type-2 particles fall towards the base. The dash-dot line corresponds to the prediction from kinetic theory for a binary mixture (Jenkins & Yoon 2002). The mismatch between the dash-dot line and the solid line is probably due to the prediction by Jenkins & Yoon (2002) being valid only for mixtures in which large particles are dilute in a dense mixture made up of smaller particles. This assumption is satisfied best in the limit of low  $\widehat{s}$  and  $\widehat{\rho}$ , which is clearly seen in the bottom left corner of figure 4. In this limit, our continuum theory is not valid, as from Savage & Lun (1988) and Thornton *et al.* (2012) it is known that for size ratios greater than 2 percolation effects are present. In our current study this corresponds to  $\widehat{s} < 0.5$  and  $\widehat{s} > 2$ . Percolation of small particles through the matrix of large particles occurs simply as a result of gravity, in the absence of shear; this is in contrast to kinetic sieving that requires the combination of gravity and shear to be active.

Felix & Thomas (2004) experimentally investigated density and size segregation for both chute flows and rotating drums. It is not possible to directly compare their chute flow results with our DPM simulations, as in their chute experiments the volume fraction of the type-2 species (tracers) is 10%. It is very hard to directly fit their experimental data to obtain the value of  $a$ ; however, several qualitative similarities can be found between our DPM simulations and their experimental findings. Firstly, for  $\widehat{s} = 1$  and  $\widehat{\rho} \approx 1.1$  they conducted two experiments, observing segregation only in

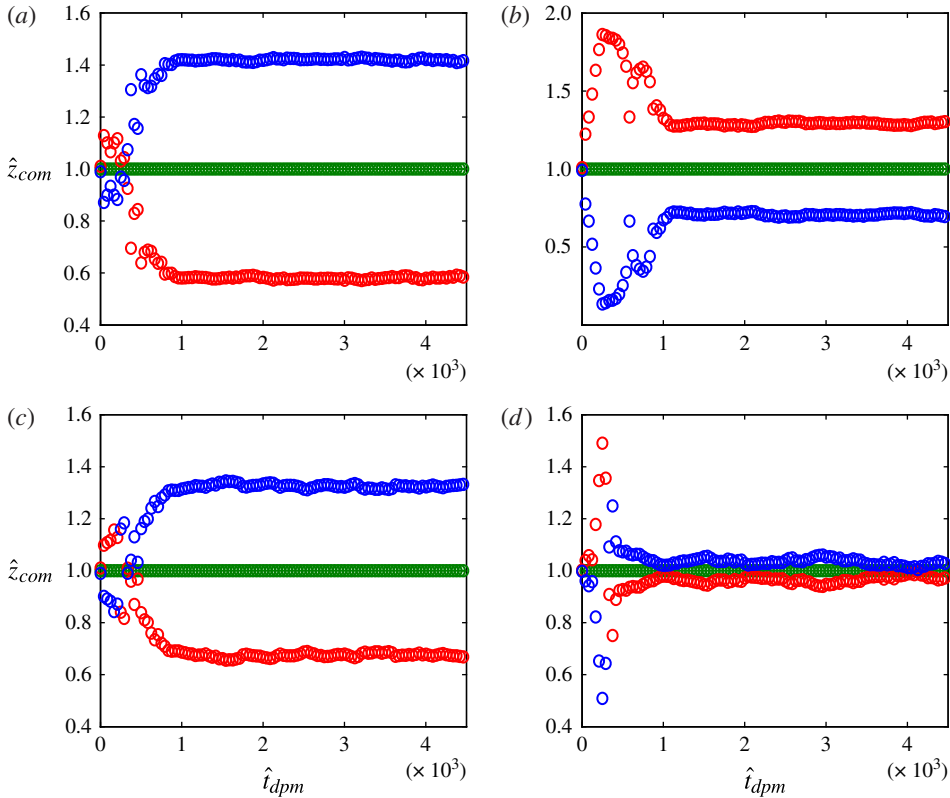


FIGURE 3. Plots against time of the  $z$ -component of the centre of mass, scaled by the vertical centre of mass of the bulk, for particle species type 1 ( $COM_1$ , red), particle species type 2 ( $COM_2$ , blue) and the bulk ( $COM_B$ , green), with parameter values (a)  $(\hat{s}, \hat{\rho}) = (1.4, 1.0)$ , (b)  $(\hat{s}, \hat{\rho}) = (1.0, 1.4)$ , (c)  $(\hat{s}, \hat{\rho}) = (1.4, 1.4)$  and (d)  $(\hat{s}, \hat{\rho}) = (0.9, 0.7)$ .

one and a homogeneous mixture state in the other, which indicates that the mixture weakly segregates at that set of ratios of size and density. For these ratios, our DPM data shows weak segregation (see figure 4), i.e. the flowing mixture only partially segregates, with a fairly homogeneous mixture still existing in the bulk (see figure 5a). We only see almost complete segregation in the regions of figure 4 with dark blue or red spots. However, as we measure the centre of mass of both species, we can detect even weak segregation; compare panels (a) and (b) of figure 5, which correspond to cases where  $\hat{D}_{com} = -0.1$  and  $0.5$ , respectively. The weak segregation in our phase plot seems to correspond to the homogeneous states of Felix & Thomas (2004), as such weak segregation could not be captured by the experimental techniques they employed. Secondly, for the cases where  $\hat{\rho} \approx 1.3$  and  $\hat{s} = (1.0, 1.1, 1.2, 1.3)$ , Felix & Thomas (2004) observed undeterminable or homogeneous mixture states, which again correspond to a weakly, not fully, segregated region in the phase plot from our DPM simulations. However, for larger size ratios, i.e.  $\hat{s} > 2$ , an opposite trend with respect to the density ratio is observed in their experiments, indicating that the segregation reverses direction. Given these differences, we suggest that this behaviour could be due to percolation effects and the different volume fractions considered; further study is required to confirm this.

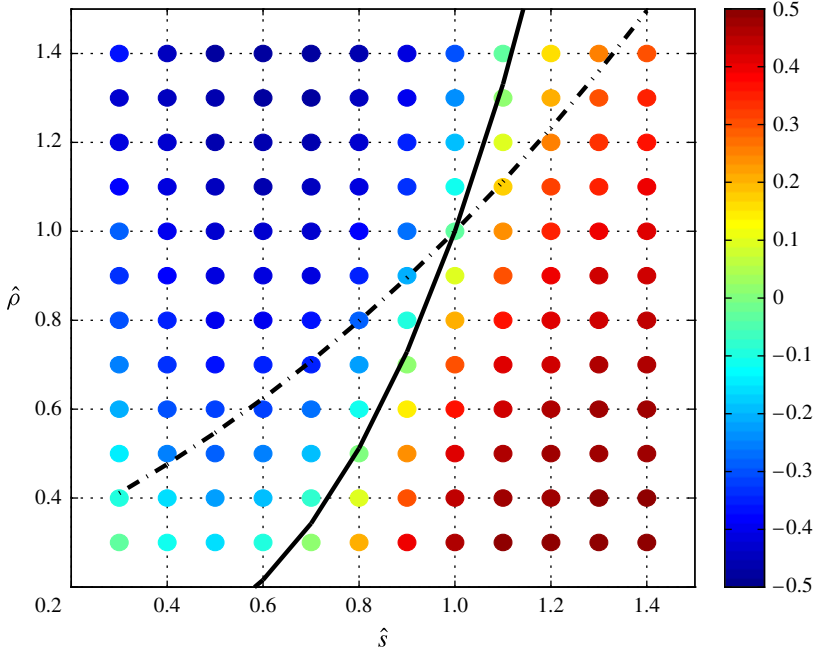


FIGURE 4. Plot of  $\widehat{D}_{com} = (COM_2 - COM_B)/COM_B$  for different values of  $\widehat{\rho}$  and  $\widehat{s}$ , with the particle volume fraction of each species type being  $\phi_i = 50\%$ . From theory, the solid line represents the weak segregation line for  $a = 3$  and the dot-dash line is the weak segregation line analytically predicted for spheres by Jenkins & Yoon (2002); in their theory, large particles are assumed to be dilute in a dense gas of small particles.

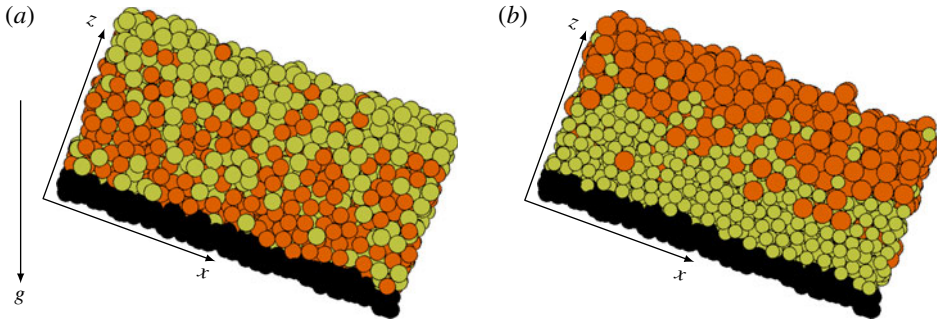


FIGURE 5. A snapshot of a bidisperse mixture flowing in a periodic box inclined at  $26^\circ$  to the horizontal, at steady state, with parameter values (a)  $(\widehat{s}, \widehat{\rho}) = (1.0, 1.1)$  and (b)  $(\widehat{s}, \widehat{\rho}) = (1.4, 1.0)$ . Colours/shades indicate the fixed base (black), species type 1 (light green) and species type 2 (orange).

Moreover, a generalised pressure scaling function could be obtained directly from the DPM simulations. This work is ongoing and some early results can be found in Weinhart *et al.* (2013). In this paper, we have not incorporated the diffusive nature of these segregating flows into our model (Gray & Chugunov 2006); therefore the model predicts full segregation, eventually, on either side of the no-segregation line. However,

if we had included diffusion in the model, then  $\hat{D}_{com}$  could be reinterpreted as a segregation Péclet number (ratio of segregation to diffusive strength) as in Thornton *et al.* (2012).

## 5. Summary and conclusions

In this paper, we focussed on bidisperse flows over inclined channels with size ratios less than 1.5. We derived a generic continuum model to predict the extent of segregation in a bidisperse granular mixture flow due to differences in particle size and density. For a given pair of density and size ratios, the model predicts the extent of demixing in gravity-driven chute flows. For purely size-based segregation, the model has been compared to two previous models. The derived model, for constant shear, is solved analytically using the method of characteristics and numerically using a discontinuous Galerkin finite element method. The model was also used to predict the ratios of particle size and density for which very weak or no segregation would occur. The prediction is independent of the details of the drag coefficient between the particles and the bulk velocity profile of the flow. To validate this prediction, we performed discrete particle simulations as an alternative to laboratory experiments of field measurements. The model performs surprisingly well when compared with the discrete particle simulations, with the fitting parameter ‘*a*’ determined from the discrete particle simulations. The advantage of our continuum model is that it permits analytical and fast numerical solutions. However, for size ratios  $\hat{s} < 0.5$  and  $\hat{s} > 2$ , the current model is not valid as percolation effects (Savage & Lun 1988; Thornton *et al.* 2012) are not accounted for.

## Acknowledgements

The authors would like to thank the Dutch Technology Foundation STW for its financial support of the project ‘Polydispersed Granular Flows through Inclined Channels’. We thank Stefan Luding and Thomas Weinhart for valuable discussions. We also thank Dinant Krijgsman and Thomas Weinhart for their assistance in the DPM simulations with the open-source code MercuryDPM.

## REFERENCES

- BOKHOVE, O. & THORNTON, A. R. 2012 Shallow granular flows. In *Handbook of Environmental Fluid Dynamics* (ed. H. J. Fernando), pp. 545–556. CRC Press.
- BRIDGWATER, J. 1976 Fundamental powder mixing mechanisms. *Powder Technol.* **15**, 215–236.
- BRITO, R. & SOTO, R. 2009 Competition of Brazil nut effect, buoyancy, and inelasticity induced segregation in a granular mixture. *Eur. Phys. J. Spec. Top.* **179**, 207–219.
- CUNDALL, P. A. & STRACK, O. D. L. 1979 A discrete numerical model for granular assemblies. *Geotechnique* **29** (1), 47–65.
- DRAHUN, J. A. & BRIDGWATER, J. 1983 The mechanisms of free surface segregation. *Powder Technol.* **36**, 39–53.
- DURAN, J. 2000 *Sands, Powders, and Grains*. Springer.
- FELIX, G. & THOMAS, N. 2004 Evidence of two effects in the size segregation process in dry granular media. *Phys. Rev. E* **70**, 051307.
- GRAY, J. M. N. T. & CHUGUNOV, V. A. 2006 Particle-size segregation and diffusive remixing in shallow granular avalanches. *J. Fluid Mech.* **569**, 365–398.
- GRAY, J. M. N. T. & THORNTON, A. R. 2005 A theory for particle size segregation in shallow granular free-surface flows. *Proc. R. Soc. A* **461**, 1447–1473.

- GRIGORIAN, S. S., EGLIT, M. E. & IAKIMOV, I. L. 1967 New statement and solution of the problem of the motion of snow avalanche. In *Snow, Avalanches & Glaciers*, Tr. Vysokogornogo Geofizich Inst., vol. 12, pp. 104–113. Vysokogornogo Geofizich Institute.
- JAIN, N., OTTINO, J. M. & LUEPTOW, R. M. 2005 Regimes of segregation and mixing in combined size and density granular systems: an experimental study. *Granul. Matt.* **7**, 69–81.
- JENKINS, J. T. & YOON, D. K. 2002 Segregation in binary mixtures under gravity. *Phys. Rev. Lett.* **88**, 194301.
- KHAKHAR, D. V., MCCARTHY, J. J. & OTTINO, J. M. 1999 Mixing and segregation of granular materials in chute flows. *Chaos* **9**, 594–610.
- LUDING, S. 2008 Introduction to discrete element methods: basic of contact force models and how to perform the micro-macro transition to continuum theory. *Eur. J. Environ. Civ. Engng* **12** (7–8), 785–826.
- MARKS, B. & EINAV, I. 2011 A cellular automaton for segregation during granular avalanches. *Granul. Matt.* **13**, 211–214.
- MARKS, B., ROGNON, P. & EINAV, I. 2012 Grainsize dynamics of polydisperse granular segregation down inclined planes. *J. Fluid Mech.* **690**, 499–511.
- MORLAND, L. W. 1992 Flow of viscous fluids through a porous deformable matrix. *Surv. Geophys.* **13**, 209–268.
- PESCH, L., BELL, A., SOLLIE, H., AMBATI, V. R., BOKHOVE, O. & VAN DER VEGT, J. J. W. 2007 hpGEM – a software framework for discontinuous Galerkin finite element methods. *ACM Trans. Math. Softw.* **33**, 23.
- POLLARD, B. L. & HENEIN, H. 1989 Kinetics of radial segregation of different sized irregular particles in rotary cylinders. *Can. Metall. Q.* **28**, 29–40.
- SAVAGE, S. B. & HUTTER, K. 1991 The dynamics of avalanches of granular materials from initiation to runout. Part I: analysis. *Acta Mechanica* **86**, 201–223.
- SAVAGE, S. B. & LUN, C. K. K. 1988 Particle size segregation in inclined chute flow of dry cohesionless granular solids. *J. Fluid Mech.* **189**, 311–335.
- SHINBROT, T., ALEXANDER, A. & MUZZIO, F. J. 1999 Spontaneous chaotic granular mixing. *Nature* **397**, 675–678.
- TASSI, P. A., BOKHOVE, O. & VIONNET, C. A. 2007 Space discontinuous Galerkin method for shallow water flows – kinetic and HLLC flux, and potential vorticity generation. *Adv. Water Resour.* **30**, 998–1015.
- THORNTON, A. R., GRAY, J. M. N. T. & HOGG, A. J. 2006 A three-phase mixture theory for particle size segregation in shallow granular free-surface flows. *J. Fluid Mech.* **550**, 1–26.
- THORNTON, A. R., WEINHART, T., LUDING, S. & BOKHOVE, O. 2012 Modeling of particle size segregation: calibration using the discrete particle method. *Intl J. Mod. Phys. C* **23**, 1240014.
- TRIPATHI, A. & KHAKHAR, D. V. 2013 Density difference-driven segregation in a dense granular flow. *J. Fluid Mech.* **717**, 643–669.
- ULRICH, S., SCHRÖTER, M. & SWINNEY, H. L. 2007 Influence of friction on granular segregation. *Phys. Rev. E* **76**, 042301.
- VOORTWIS TE, A. 2013 Closure laws for granular, shallow-layer, bi-dispersed flows down an inclined chute. Master thesis, Multi Scale Mechanics Group, Mechanical Engineering Faculty of Engineering Technology, Universiteit Twente (§ 3.2.4).
- WEINHART, T., LUDING, S. & THORNTON, A. R. 2013 From discrete particles to continuum fields in mixtures. *AIP Conf. Proc.* **1542**, 1202–1205.
- WEINHART, T., THORNTON, A. R., LUDING, S. & BOKHOVE, O. 2012 Closure relations for shallow granular flows from particle simulations. *Granul. Matt.* **14** (4), 531–552.
- WHITHAM, G. B. 1974 *Linear and Nonlinear Waves*. John Wiley & Sons.
- WIEDERSEINER, S., ANDREINI, N., ÉPELY-CHAUVIN, G., MOSER, G., MONNEREAU, M., GRAY, J. M. N. T. & ANCEY, C. 2011 Experimental investigation into segregating granular flows down chutes. *Phys. Fluids* **23**, 013301.
- WOODHOUSE, M. J., THORNTON, A. R., JOHNSON, C. G., KOKELAAR, B. P. & GRAY, J. M. N. T. 2012 Segregation-induced fingering instabilities in granular free-surface flows. *J. Fluid Mech.* **709**, 543–580.